First submission

Editor guidance

Please submit by **23 May 2018** for the benefit of the authors (and your $200 publishing discount).

✓ Structure and Criteria
Please read the 'Structure and Criteria' page for general guidance.

❗ Custom checks
Make sure you include the custom checks shown below, in your review.

▦ Raw data check
Review the raw data. Download from the materials page.

🖼 Image check
Check that figures and images have not been inappropriately manipulated.

Privacy reminder: If uploading an annotated PDF, remove identifiable information to remain anonymous.

Files
Download and review all files from the materials page.

5 Figure file(s)
5 Table file(s)

❗ Custom checks

Vertebrate animal usage checks

❗ Have you checked the authors ethical approval statement?

❗ Were the experiments necessary and ethical?

❗ Have you checked our animal research policies?

Structure and Criteria

Structure your review

The review form is divided into 5 sections.
Please consider these when composing your review:

1. **BASIC REPORTING**
2. **EXPERIMENTAL DESIGN**
3. **VALIDITY OF THE FINDINGS**
4. General comments
5. Confidential notes to the editor

📄 You can also annotate this PDF and upload it as part of your review

When ready [submit online](#).

Editorial Criteria

Use these criteria points to structure your review. The full detailed editorial criteria is on your [guidance page](#).

BASIC REPORTING

- Clear, unambiguous, professional English language used throughout.
- Intro & background to show context. Literature well referenced & relevant.
- Structure conforms to [PeerJ standards](#), discipline norm, or improved for clarity.
- Figures are relevant, high quality, well labelled & described.
- Raw data supplied (see [PeerJ policy](#)).

EXPERIMENTAL DESIGN

- Original primary research within [Scope of the journal](#).
- Research question well defined, relevant & meaningful. It is stated how the research fills an identified knowledge gap.
- Rigorous investigation performed to a high technical & ethical standard.
- Methods described with sufficient detail & information to replicate.

VALIDITY OF THE FINDINGS

- Impact and novelty not assessed. Negative/inconclusive results accepted. *Meaningful* replication encouraged where rationale & benefit to literature is clearly stated.
- Data is robust, statistically sound, & controlled.
- Conclusions are well stated, linked to original research question & limited to supporting results.
- Speculation is welcome, but should be identified as such.

Standout reviewing tips

The best reviewers use these techniques

Tip	Example
Support criticisms with evidence from the text or from other sources	*Smith et al (J of Methodology, 2005, V3, pp 123) have shown that the analysis you use in Lines 241-250 is not the most appropriate for this situation. Please explain why you used this method.*
Give specific suggestions on how to improve the manuscript	*Your introduction needs more detail. I suggest that you improve the description at lines 57- 86 to provide more justification for your study (specifically, you should expand upon the knowledge gap being filled).*
Comment on language and grammar issues	*The English language should be improved to ensure that an international audience can clearly understand your text. Some examples where the language could be improved include lines 23, 77, 121, 128 – the current phrasing makes comprehension difficult.*
Organize by importance of the issues, and number your points	*1. Your most important issue* *2. The next most important item* *3. ...* *4. The least important points*
Please provide constructive criticism, and avoid personal opinions	*I thank you for providing the raw data, however your supplemental files need more descriptive metadata identifiers to be useful to future readers. Although your results are compelling, the data analysis should be improved in the following ways: AA, BB, CC*
Comment on strengths (as well as weaknesses) of the manuscript	*I commend the authors for their extensive data set, compiled over many years of detailed fieldwork. In addition, the manuscript is clearly written in professional, unambiguous language. If there is a weakness, it is in the statistical analysis (as I have noted above) which should be improved upon before Acceptance.*

The effects of growth rate and biomechanical loading on bone laminarity within the emu skeleton

Amanda L Kuehn [1] , Andrew H Lee [2] , Russell P Main [3] , Erin LR Simons [Corresp. 2]

[1] Arizona College of Osteopathic Medicine, Midwestern University, Glendale, AZ, United States

[2] Department of Anatomy, Arizona College of Osteopathic Medicine, College of Veterinary Medicine, Midwestern University, Glendale, AZ, United States

[3] College of Veterinary Medicine, Purdue University, West Lafayette, IN, United States

Corresponding Author: Erin LR Simons
Email address: esimon@midwestern.edu

The orientation of vascular canals in primary bone may reflect differences in growth rate and/or adaptation to biomechanical loads. Previous studies link specific canal orientations to bone growth rates, but results between different taxa are contradictory. Circularly-oriented vascular canals (forming laminar bone) have been hypothesized to reflect either (or both) rapid growth rate or locomotion-induced torsional loading. Previous work on the hindlimb biomechanics in the emu shows that the femur and tibiotarsus experience large shear strains, likely resulting from torsional loads, that increase through ontogeny. Here, we test how growth rate and biomechanical loading affect bone laminarity in wing and hindlimb elements from growing emu (2 - 416 wks). If bone laminarity is purely an expression of growth rate, it should be most elevated at the growth spurt and decrease with age at a time when shear strains increase in the emu femur and tibiotarsus. Alternatively, if laminar bone reflects biomechanical accommodation, it should become more abundant with age. Transverse mid-shaft histological sections from the limb bones (femur, tibiotarsus, humerus, ulna, and radius) were prepared and imaged. Growth rates were measured using fluorescent bone labels. Vascular canal orientation was quantified using laminarity index (proportion of circularly oriented canals). Growth rates were found to be highest in young individuals for all five skeletal elements. Laminarity significantly decreased with increasing growth rate in hindlimb elements, but no relationship was seen between laminarity and growth rate in forelimb elements. In the femur and tibiotarsus, laminarity significantly increased with increasing shear strain, which supports the hypothesis that laminar bone is a feature of torsionally loaded bone. A moderate amount of bone laminarity was found in the humerus and ulna, despite emu wings being vestigial and likely to experience minimal biomechanical loading, suggesting that laminar bone may in some cases be a retained ancestral feature. In conclusion, torsional loading appears to have a greater impact on vascular canal orientation than growth rate in the femur and

tibiotarsus of the emu.

1   **The effects of growth rate and biomechanical loading on bone laminarity within the emu**

2   **skeleton**

3

4   **Amanda L. Kuehn[1], Andrew H. Lee[2], Russell P. Main[3], Erin L. R. Simons[2]**

5

6   [1]Arizona College of Osteopathic Medicine, Midwestern University, Glendale, AZ, USA

7   [2]Department of Anatomy, Arizona College of Osteopathic Medicine, College of Veterinary

8   Medicine, Midwestern University, Glendale, AZ, USA

9   [3]College of Veterinary Medicine, Purdue University, West Lafayette, IN, USA

10

11   Corresponding Author:

12   Erin Simons[1]

13

14   Email address: esimon@midwestern.edu

15

16

17

18

19

20

21

22

23

24   **ABSTRACT**

25   The orientation of vascular canals in primary bone may reflect differences in growth rate

26   and/or adaptation to biomechanical loads. Previous studies link specific canal orientations to

27   bone growth rates, but results between different taxa are contradictory. Circularly-oriented

28   vascular canals (forming laminar bone) have been hypothesized to reflect either (or both) rapid

29   growth rate or locomotion-induced torsional loading. Previous work on the hindlimb

30   biomechanics in the emu shows that the femur and tibiotarsus experience large shear strains,

31   likely resulting from torsional loads, that increase through ontogeny. Here, we test how growth

32   rate and biomechanical loading affect bone laminarity in wing and hindlimb elements from

33   growing emu (2 - 416 wks). If bone laminarity is purely an expression of growth rate, it should

34   be most elevated at the growth spurt and decrease with age at a time when shear strains increase

35   in the emu femur and tibiotarsus. Alternatively, if laminar bone reflects biomechanical

36   accommodation, it should become more abundant with age. Transverse mid-shaft histological

37   sections from the limb bones (femur, tibiotarsus, humerus, ulna, and radius) were prepared and

38   imaged. Growth rates were measured using fluorescent bone labels. Vascular canal orientation

39   was quantified using laminarity index (proportion of circularly oriented canals). Growth rates

40   were found to be highest in young individuals for all five skeletal elements. Laminarity

41   significantly decreased with increasing growth rate in hindlimb elements, but no relationship was

42   seen between laminarity and growth rate in forelimb elements. In the femur and tibiotarsus,

43   laminarity significantly increased with increasing shear strain, which supports the hypothesis that

44   laminar bone is a feature of torsionally loaded bone. A moderate amount of bone laminarity was

45   found in the humerus and ulna, despite emu wings being vestigial and likely to experience

46   minimal biomechanical loading, suggesting that laminar bone may in some cases be a retained

47 ancestral feature. In conclusion, torsional loading appears to have a greater impact on vascular

48 canal orientation than growth rate in the femur and tibiotarsus of the emu.

49

50 **INTRODUCTION**

51   Avian bone tissue is highly vascularized with a fibrolamellar structure, which allows for

52 rapid growth by depositing randomly arranged woven bone initially, then filling in with stronger

53 more organized lamellar bone (Curry, 2002). Primary osteons are deposited around central canals

54 that house blood vessels and nerves. These vascular canals vary in orientation and bones can be

55 classified based on the predominant canal orientation. Laminar bone has an abundance of

56 circular canals, those that in a bone cross section are oriented parallel to the periosteal surface of

57 the bone. Additional canal orientations include: radial, those orthogonal to the periosteal surface;

58 longitudinal, those running parallel to the long axis of the bone; and oblique, all other

59 orientations (de Ricqlès et al., 1991). Avian bone tissue largely retains its primary structure

60 throughout growth and adulthood (Enlow and Brown, 1957). It has been hypothesized that

61 differences in primary vascular canal orientation might be a reflection of the functional demands

62 placed on the bone, growth rate, or phylogenetic relationships.

63   Amprino (1947) first suggested that the organization of bone microstructure may be

64 influenced by bone growth rate, such that woven bone is deposited during rapid growth and

65 lamellar bone during slow growth (de Ricqlès et al., 1991). Further studies have investigated

66 whether specific primary vascular canal orientations in fibrolamellar bone are also associated

67 with slow or fast growth by directly comparing microstructure with bone growth rates measured

68 through the use of injectable fluorochromes (Castanet et al., 2000; de Margerie, 2002; de

69 Margerie et al., 2004). Rapidly growing hindlimb bones of ratites have been found to exhibit

70 structure that is laminar and reticular (bone with an abundance of obliquely oriented canals)

71 (Castanet et al., 2000), whereas the much slower growing wing elements of the ratites exhibit

72 reticular and longitudinal canal structure. This suggests that laminar bone, in part, may reflect

73 faster growth rates. This result was supported in a recent study of pigeon wing elements, which

74 showed that peak laminarity (proportion of laminar bone) coincides with the growth spurt in each

75 element (Ourfalian, Ezell & Lee, 2016). However, work on mallard long bones showed no

76 relationship between growth rate and predominant vascular canal orientation (de Margerie,

77 2002). And in the king penguin, radially-oriented canals dominated in the fastest growing

78 sections, not circular canals (laminar bone) as was hypothesized. (de Margerie et al., 2004).

79 Likewise, chickens selected for fast growth showed tibiotarsi with more radial canals (Williams

80 et al., 2004).

81   Laminar bone has been hypothesized to better resist torsional loading. In laminar bone,

82 the bone tissue is arranged in 'sheets' or 'plates' between layers of circular canals. Shear strain is

83 thought to flow continuously within these 'sheets', and thus the concentrated stresses on the bone

84 tissue surrounding the canals is reduced (de Margerie et al., 2004). Indeed, elements that are

85 predominantly experiencing torsional loads have been found to exhibit laminar bone. Laminar

86 bone is found to be most abundant in the humerus, ulna, and femur in a large sample of flighted

87 bird species (de Margerie, 2002; de Margerie et al., 2005). *In vivo* strain gauge studies have

88 shown that at least two of these elements, the humerus in the pigeon during flapping flight and

89 the femur in the chicken and emu during terrestrial running, experience predominantly torsional

90 loads (Biewener and Dial, 1995; Carrano and Biewener, 1999; Main and Biewener, 2007).

91 Changes in posture affect the amount of torsion experienced, such that when the center of mass

92 of white leghorn chickens was modified, the femur experienced higher torsional loads due to its

93   more horizontal orientation. In addition, it has been hypothesized that specific wing shape and

94   the locomotor style associated with it may affect how much torsional load is placed on limb

95   elements. For example, laminarity in the humerus of birds that utilize flapping and static soaring

96   is higher than in the humerus of birds that use dynamic soaring (de Margerie et al, 2005; Simons

97   and O'Connor, 2012).

98   A limitation of previous studies of laminar bone is the indirect comparison of bone

99   histology in one species with bone growth rates and/or *in vivo* strain gauge measures taken from

100   different species. In this study, we present an analysis of laminar bone in a species in which bone

101   growth rate and *in vivo* bone strain data were directly measured. The emu (*Dromaius*

102   *novaehollandiae,* Order Struthioniformes, Family Dromaiidae) is a flightless bird endemic to

103   Australia, but widely farmed in the US. The individuals included in this study comprise a growth

104   series that were previously injected with fluorescent bone labels and surgically implanted with

105   gauges to measure *in vivo* locomotor strains in the femur and tibiotarsus (Main and Biewener,

106   2007). These strains were predominantly shear (produced by torsional loads) and increased from

107   juveniles to adults (Main and Biewener, 2007). Although the wings of these individuals were not

108   measured for bone strain, they are extremely reduced and have no known function other than

109   being raised to aid thermoregulation (del Hoyo et al., 1992; Maxwell and Larsson, 2007).

110   Presumably, shear strains are negligible in the wing elements. Therefore, if laminarity is an

111   adaptation to torsion-induced shear strains, we predict that hindlimb bone laminarity will

112   increase from juveniles to adults. Moreover, we expect little to no laminar bone in the vestigial

113   wing elements. Alternatively, if bone laminarity reflects rapid growth, it should be abundant in

114   juveniles and decrease with age as growth slows in adults. In addition, hindlimb elements in emu

115   grow at a faster rate than wing elements (Castanet et al., 2000), so we predict overall greater

116   laminarity in hindlimb than forelimb elements. Having access to growth rate measurements,

117   direct biomechanical data, and direct histological work to classify laminarity makes this study a

118   first of its kind that will be able to clarify which factors have the most impact on vascular canal

119   orientation in emu limbs.

120

121   **MATERIALS & METHODS**

122   This study samples forelimb and hindlimb elements from ten emus ranging in age from 2

123   to 416 weeks (Table 1). Birds used in this study were euthanized as part of a previous study

124   (Main and Biewener, 2007) and the selected elements stored frozen. Emus were originally

125   obtained as hatchlings by R.P. Main (at the time at Harvard University) from commercial farms

126   (Songline Emu Farm, Gill, MA, USA; Scattered Oaks Emu Farm, Iola, TX, USA; Deep Hollow

127   Farm, Oakdale, CT, USA) and raised at Harvard University's Concord Field Station (Bedford,

128   MA, USA)(Harvard FAS IACUC AEP 23-15). For the first eight weeks of life the emus were

129   held in indoor enclosures, and then moved into large outdoor enclosures. All birds had free

130   access to commercial ratite diet (Mazuri, PMI Nutrition International, LLC, Brentwood, MO,

131   USA) and water. Male and female birds were included based on availability. Emus exhibit a

132   minor degree of sexual dimorphism, with females being slightly larger on average (del Hoyo et

133   al., 1992). The difference in size is not large enough to be considered a confounding factor for

134   this study.

135   As a part of a previous study (Main and Biewener, 2007), each bird was given a single

136   intramuscular injection of xylenol orange (80mg/kg) followed by calcein (30mg/kg) according to

137   an injection schedule. Injections were given one week apart in birds less than 16 weeks of age,

138   two weeks apart in birds between 16 and 65 weeks of age, and four weeks apart in birds older

139   than 65 weeks. Xylenol and calcein are fluorescent labels that incorporated rapidly into newly

140   mineralizing surfaces of bone at the time of injection (An and Martin, 2003). Thus, the time

141   elapsed and the space between xylenol and calcein labels allows the calculation of periosteal

142   (radial) growth rate. One week after the last injection, surgery was performed to attach strain

143   gauges to the cranial, caudal, and lateral aspects of the left femur and the cranial, caudal, and

144   medial aspects of the left tibiotarsus. Single element strain gauges were used on the lateral femur

145   and cranial and medial tibiotarsus. Rectangular rosette gauges were used on the cranial and

146   caudal femur and caudal tibiotarsus. Rosette strain gauges allow both tensile and compressive

147   principal strains and their orientations to be measured, and were placed so the central element of

148   the gauge was parallel to the long axis of the bone. One day after surgery, the birds were run on a

149   treadmill over a wide range of speeds and gaits. The raw data produced from the strain gauges

150   was converted from voltages into microstrain using a custom MATLAB program. Shear strains

151   were calculated from the rosette strain gauges using standard equations (Biewener and Dial,

152   1995). High quality shear strain data were most consistently collected from the caudal cortices of

153   the femur and tibiotarsus and that is what is reported here. Trials in which the birds ran with a

154   duty factor near 0.50 are included in the shear strain analysis (mean ± SD: 0.50 ± 0.02). Each

155   trial was represented by five footfalls and, generally, two trials were collected for each bird.

156   Following bone strain data collection, animals were euthanized. After death, whole wings were

157   removed from the individuals and stored frozen. Histological sections of the femora and

158   tibiotarsi were prepared (see Main and Biewener, 2007 for details) and shipped with the frozen

159   wings to Midwestern University.

160   **Histological Preparation**

161   Emu wings were thawed and feathers, skin, muscles, and tendons were reflected to

162 expose the skeletal elements. Both right and left wings were used based on availability. Using

163 digital calipers, total length of each bone was measured and recorded. A 37-mm segment was

164 removed using a Dremel tool from the mid-shaft region of the humerus, ulna, and radius. For two

165 and four week old individuals whole elements were harvested due to their small size. Segments

166 were marked to maintain orientation. Dissected bone segments were placed in 10% neutral

167 buffered formalin for fixation, then dehydrated in a graded ethanol series (70%, 85%, 100%)

168 under vacuum. Segments were cleared with a xylene-substitute (Histo-clear; National

169 Diagnostics, Atlanta, Georgia, USA). The bone segments were then vacuum- infiltrated and

170 embedded in glass vials using Osteo-Bed Plus Resin, a two-part methyl methacrylate

171 (Polysciences Inc.). Vials were placed in a 32˚ C bead bath to fully harden.

172   Once the resin hardened, vials were broken and two roughly 800-um transverse sections

173 were cut using a diamond blade saw (Isomet 1000; Buehler, Lake Bluff, Illinois, USA). These

174 sections were glued onto frosted glass slides using two-ton epoxy (Devcon, Milpitas, California,

175 USA), keeping consistent spatial orientation. Slides were then ground to a thickness of

176 100±10um using a graded scale of grit paper on a stand grinder (Metaserv 250; Buehler, Lake

177 Bluff, Illinois, USA) and coverslipped with Permount (Fisher Scientific). The histological

178 preparation was modified from An and Martin (2003) and closely followed Lee and Simons

179 (2015).

180 **Image Collection**

181   The undecalcified sections contain xylenol (orange) and calcein (green) fluorochromes

182 that were incorporated into newly mineralizing bone at the time of injection (see above for

183 injection schedule). These fluorochromes create stable long lasting tags (van Gaalen et al., 2010)

184 and were examined under bright-field and fluorescent illumination with a motorized

185   epifluorescent microscope (IX73, Olympus). The xylenol (orange) and calcein (green) tags were

186   revealed using the TRITC and FITC filter cubes, respectively, and a multichannel (red, green,

187   bright-field) image of each section was generated with imaging software (cellSens, Olympus).

188   Sufficient optical resolution (10X UPlanAPO ≈ 0.84 µm; 20X UPlan S-APO ≈ 0.45 µm) allowed

189   the dual color-monochrome camera (DP80, Olympus) to capture high quality images (10X =

190   1.02 µm/pixel; 20X = 0.51 µm/pixel).

191   **Data Analysis**

192   Bright-field and fluorescent images were obtained from the wing and hindlimb elements

193   (Figs. 1 and 2) and divided into equal octants from the estimated bone centroid. Four octants

194   representing the cardinal anatomical positions (wing elements: cranial, caudal, dorsal, ventral;

195   hindlimb elements: cranial, caudal, lateral, medial) were extracted. Using ImageJ, each extracted

196   octant was then uncurved using the "Straighten" function. The purpose of straightening was to

197   standardize the periosteal tangent line so that appropriate measurements could be made in

198   classifying the orientation of the vascular canals (Lee and Simons, 2015). To ensure there was

199   minimal deformation of the image during the straightening process, known test angles were

200   placed upon the image and measured in relation to the periosteal surface after the straightening

201   function had been applied. Only those images with an average deformation less than or equal to

202   10° were accepted.

203   Within each of the four octants, the calcein green and xylenol orange tags were outlined

204   with two reference lines. The distance between reference lines was measured at 10 random

205   points in each octant. Growth rate was measured by taking the mean distance between

206   consecutive fluorescent tags divided by number of days between injections (Fig. 2).

207   Degree of laminarity (Laminarity Index, LI) for each octant was assessed in two distinct

208   sample areas. To address the growth hypothesis, laminarity was measured in the area between

209   the fluorochrome reference lines in all four octants. To address the biomechanical hypothesis,

210   laminarity was measured in four sample boxes (1.5 x 1.5 mm each) placed in the caudal bone

211   cortex to represent the entire bone cortex (hindlimbs only). To measure laminarity, an ellipse was

212   drawn in each primary vascular canal in the designated sample area of the straightened octant.

213   The angle at which the ellipse sat in relation to the straightened periosteal surface was measured.

214   We used the criteria set forth by de Margerie (2002) to classify the orientation of the vascular

215   canals: (1) circular canals are oriented parallel ($0° \pm 22.5°$) to the periosteal surface of the bone;

216   (2) radial canals are orthogonal ($90 \pm 22.5°$) to the periosteal surface; (3) longitudinal canals run

217   parallel to the long axis of the bone and have ellipses with an aspect ratio of less than 3; (4)

218   oblique canals are all other orientations. Only primary vascular canals were measured. Any

219   secondary osteons in the sample area were excluded. Laminarity index (proportion of circular

220   canals to the total number of canals) was calculated using the Wilson estimate account for bias

221   from small sample sizes (Lee and Simons, 2015).

222   Statistical analyses were performed using R (R Development Team, 2017). Logistic

223   regression was used because laminarity index is a proportion and may not be normally

224   distributed; logistic regression relaxes the assumption that the data are normally distributed

225   (Warton and Hui, 2011; Ourfalian, Ezell & Lee, 2016). To test the growth hypothesis, we

226   performed logistic regression between laminarity indices of each bone and growth rate. To test

227   for correlation between laminarity and shear strain, we focused on the data obtained from the

228   caudal cortex in the femur and tibiotarsus. Average laminarity indices from the four sample

229   boxes placed in the caudal octant of the hindlimb elements for each bird were logistically

230   regressed against a mean for the caudally measured shear strains from two experimental trials,

231 previously collected by Main and Biewener (2007).

232

233 **RESULTS**

234 Measured growth rates ranged from 1.33 um/day (radius of 48 week old individual) to

235 162.62 um/day (femur of 4.6 week old individual) (Table 2). Negligible growth was recorded in

236 the eight-year-old individuals. Laminarity indices range from 0.02 to 0.58 as measured for the

237 growth hypothesis (Table 2) and 0.03 to 0.79 as measured for the biomechanical hypothesis

238 (Table 3).

239 Logistic regression between LI and growth rate (GR) showed a significant negative

240 relationship in the femur (p<0.001) and tibiotarsus (p<0.001) (Fig. 3, Table 2). No significant

241 relationship was found between laminarity and growth rate in wing elements (Fig. 4, humerus:

242 p=0.08, ulna: p=0.29, radius: p=0.52).

243 Logistic regression between caudal octant LI and shear strain showed a significant

244 positive relationship in both the femur (p < 0.001) and tibiotarsus (p<0.001) (Fig. 5, Table 3).

245

246 **DISCUSSION**

247 **Does bone laminarity reflect fast growth?**

248 The fastest growth rate in all elements was found in the 4.6-week old individual (Table

249 2). As expected, hindlimb elements had higher growth rates than forelimb elements, reaching a

250 maximum of 163 um/day in the femur and 99 um/day in the tibiotarsus. The humerus grew the

251 fastest of the wing elements, reaching a maximum rate of 25 um/day measured in the 2.3 and 4.6

252 week old individual. Birds older than 8 weeks experienced a drastic decrease in bone growth rate

253 in both hindlimb and forelimb elements. Previous analysis of emu somatic growth rate showed

254 the maximum velocity of growth (inflection point) to be about 15-17 weeks of age

255 (Goonewardene et al., 2003). Our results suggest maximum bone growth occurs much earlier

256 (about 5 weeks) and is not an accurate proxy for the somatic growth inflection.

257   There was a significant negative relationship between bone laminarity and growth rate in

258 both hindlimb elements (Fig. 3). In the hindlimb, the lowest laminarity was found in the

259 youngest birds, where the growth rate was the fastest. This is consistent with findings in the king

260 penguin that also reported laminar bone to be associated with slower growth rates in four limb

261 bones: femur, tibiotarsus, humerus, and radius (de Margerie et al., 2004). Notably, our results

262 differ from those previously reported for young emu bones in which laminar and reticular bone

263 was found in the fastest growing hindlimb bones (Castanet et al., 2000). In particular, Castanet et

264 al. (2000) found laminar bone to be most abundant in the femur and tibiotarsus of emu less than

265 2 months of age, which corresponds to the youngest individuals in our study. The emus included

266 in our study grew in mass about 3 times faster than the emus in the Castanet et al. (2000) study.

267 If laminarity is associated with slower growth rates, the youngest emus we studied may have

268 been growing too fast for laminar bone to form. In contrast, Castanet et al. (2000) found reticular

269 bone to be more abundant in the humerus. Our study did not specifically address reticular bone,

270 but by taking the proportion of oblique vascular canals (a "reticular index"), we found the

271 amount of reticular bone in the fastest growing individual to be low in the hindlimb elements

272 (femur and tibiotarsus: 0.17), and moderate to high in the wing elements (humerus: 0.62, ulna:

273 0.58, radius: 0.45). This result is, at least, consistent with the previous study. The data analysis in

274 the earlier emu study (Castanet et al., 2000) was conducted before a more rigorous method for

275 measuring vascular canals was developed (de Margerie, 2002), which may also affect differences

276 seen between the two separate emu populations. Regardless, the results of the direct laminarity

277   indices and growth rates measured here do not support the hypothesis that high laminarity

278   reflects rapid growth in the emu.

Does bone laminarity reflect biomechanical load?

280   Within the caudal octants of the hindlimb elements, we found a positive correlation

281   between laminarity and shear strain (Fig. 5). This result supports the hypothesis that laminar

282   bone may reflect a specific type of biomechanical load - torsion. The amount of shear strain

283   occurring at the midshaft of the emu femur and tibiotarsus has been found to significantly

284   increase with age by 2-3 times, whereas body mass increases by 46 times. Laminar bone, in

285   combination with increased bone mineralization and decreased bone curvature during growth,

286   may help mitigate shear strains despite the large increase in mass (Main and Biewener, 2007).

287   Our results support the hypothesis that laminar bone is a feature of torsionally loaded

288   bone and strengthens the premise that bone histology can be used to estimate the degree of shear

289   strain experienced by bones during different types of locomotion, such as flight modes (de

290   Margerie et al., 2005; Simons and O'Connor, 2012). Although strain gauge technology is

291   improving, shear strains are not easily measured for some types of locomotion, especially flight.

292   In addition, this correlation between laminarity and shear strain could help researchers better

293   understand locomotive patterns of extinct animals that are closely related to Aves, such as other

294   extinct maniraptorans (the clade of dinosaur that includes birds). Not all members of the

295   maniraptoran clade were flighted animals (Makovicky and Zanno, 2011), but as one moves up

296   the phylogeny from non-flighted to flighted animals we may expect to see an increase in

297   laminarity within at least the humerus an adaptation to the larger expected torsional loads

298   experienced during active flight. Indeed, the humerus of Archaeopteryx appears to have

299   predominately longitudinal canals despite having cross-sectional geometry similar to birds that

300   use active flapping (Voeten et al., 2018), but further up the paravian tree, *Confuciusornis* shows

301   laminar-reticular bone in the humerus (de Ricqles et al. 2003).

302   However, this histological proxy for torsional load should be used with caution. Previous

303   studies have shown that when wings have the same general shape, laminarity in wing bones is

304   similar despite differences in primary flight mode (Simons and O'Connor, 2012; Marelli and

305   Simons, 2014). In addition, preferred flight mode may only have subtle effects on overall

306   loading of the bones, with the dominant loads being the high strains present during take-off

307   (Biewener and Dial, 1995). There is also at least one example of a bone loaded in predominantly

308   torsion that does not exhibit laminar bone. The humeri of bats show an absence of laminar bone

309   despite being loaded in torsion during flapping flight, presumably due to the slow somatic

310   growth rates of bats (Swartz, Bennet & Carrier, 1992; Lee and Simons, 2015). Additionally,

311   laminar bone may be present in the absence of dominant torsional loads. The radius of the goat

312   qualitatively appears laminar during growth and early adulthood despite experiencing

313   predominantly bending loads (Main, 2007).

314   The mean laminarity across all ages of emu was statistically larger for the femur (0.41)

315   than the tibiotarsus (0.28, p=0.007). Generally, the femur has also been shown to experience a

316   larger magnitude of shear strain than the tibiotarsus (Main and Biewener, 2007). Both elements

317   exhibited a large degree of variation, with the laminarity indices of the femur ranging from 0.02 -

318   0.56 and the tibiotarsus from 0.02 - 0.58 through ontogeny (Table 2). Interestingly, in the

319   tibiotarsus, a wide range of variation in laminarity can be seen for similar shear strain values

320   (Fig. 5). Laminarity measured on a histological section is a 2-dimensional representation of a 3-

321   dimensional meshwork of vascular canals in cortical bone. This research is limited by the

322   assumption that one or two closely placed mid-shaft histological sections are an accurate

323   representation of vascular canal structure. Future studies should incorporate new methods, such

324   as microCT (e.g., Pratt and Cooper, 2017), to assess how well laminarity measured on

325   histological sections represents actual biological structure.

326   Although there is no direct biomechanical data for the forelimb elements of these birds,

327   the wing elements presumably experience minimal loading. The emu wing is extremely reduced

328   in size, even when compared to other ratites, and no wing function has been observed except to

329   be raised for thermoregulation (del Hoyo et al., 1992). Wing muscles of emu are primarily slow

330   acting tonic muscle fibers that may not allow much wing movement (Maxwell and Larsson,

331   2007), which suggests the underlying wing elements would experience minimal biomechanical

332   loading. Interestingly, despite the assumption that the emu wing is under minimal load, a

333   moderate to high degree of laminarity was found in at least the humerus and ulna (Table 2).

334   Within the paleognaths, it has been hypothesized that at least three independent flight

335   losses have occurred, with only one order (the tinamous) still retaining the ability (Harshman et

336   al., 2008; Mitchell et al., 2014). The moderate/high wing bone laminarity may be a feature of the

337   flighted common ancestor of paleognaths that is retained in the flightless descendants. Indeed,

338   significant phylogenetic signal has been found in some osteohistological features in a sample of

339   paleognaths (Legendre et al., 2014). Future studies should investigate the histological and *in vivo*

340   loading of the flighted relatives of emus to better understand the potential influence of phylogeny

341   on bone laminarity.

342

343   **CONCLUSIONS**

344   For the emu skeleton, torsional loading appears to have a greater impact on vascular

345   canal orientation than growth rate. The increase of laminarity with increasing shear strain

346   suggests that laminar bone may be an adaptation to resist torsional loads in the femur and

347   tibiotarsus. For the humerus and ulna, moderate to high laminarity may have been inherited from

348   a flighted ancestor. Future studies should investigate laminarity in other palaeognathous birds to

349   better understand the interplay among phylogeny, ontogeny, and torsional loading on bone

350   laminarity. Other future work should focus on the experimental manipulation of biomechanical

351   loads to observe the effects on vascular canal orientation in limb bones. This could be done using

352   a similar study design, but with the addition of individuals that have been weighted (to increase

353   normal biomechanical loads) and/or undergone limb immobilization (to reduce normal

354   biomechanical loads) to better understand to what extent the amount of torsional load has on the

355   development of limb bone laminarity.   It is also important that variation found between different

356   populations be addressed and studied further. Emu body mass growth rates vary among

357   populations (e.g. Goonewardene et al., 2003), but it is unknown if bone histology also varies

358   with geography.

359

360   **ACKNOWLEDGEMENTS**

366

367

368   **REFERENCES**

369   Amprino R. 1947. La structure du tissu osseux envisagee comme expression de differences dans

370   lavitesse de l'accroissement. *Archives de Biologie* 58:315–330.

371   An YH, Martin KL. 2013. *Handbook of histology methods for bone and cartilage.* Humana

372   Press; 1st edition.

373   Biewener AA, Dial KP. 1995. In vivo strain in the humerus of pigeons (*Columba livia*). *Journal*

374   *of Morphology* 225:61–75. DOI 10.1002/jmor.1052250106.

375   Buckwalter JA, Glimcher MJ, Cooper RR, Recker R. 1995. Bone biology. *Journal of Bone and*

376   *Joint Surgery.* 77(8):1256-1275.

377   Burnham KP, Anderson DR. 2002. *Model Selection and Multimodel Inference: A Practical*

378   *Information-Theoretic Approach*, 2nd edition. Springer-Verlag, New York, 488 pp.

379   Carrano MT, and Biewener AA. 1999. Experimental alteration of limb posture in the chicken

380   (*Gallus gallus*) and its bearing on the use of birds as analogs for dinosaur locomotion.

381   *Journal of Morphology* 240(3):237-249.

382   Castanet J, Curry-Rogers K, Cubo J, Boisard JJ. 2000. Periosteal bone growth rates in extant

383   ratites (ostriche [sic] and emu). Implications for assessing growth in dinosaurs. *Comptes*

384   *Rendus de l'Academie des Sciences Serie III Sciences de la Vie* 323:543-550. DOI

385   10.1016/S0764-4469(00)00181-5.

386   Curry JD. 2002. *Bones: Structure and Mechanics*. Princeton and University Press.

387   de Ricqlès AJ. 1975. Recherches paléohistologiques sur les os longs des Tétrapodes. VII : Sur la

388   signification fonctionnelle et l'histoire des tissus osseux des Tétrapodes. *Annales de*

389   *Paléontologie.* (Vert.) 61:51–129.

390   de Ricqlès AJ, Meunier FJ, Castanet J, Francillon-Vieillot H. 1991. Comparative microstructure

391   of bone. In: Hall BK, ed. *Bone, volume 3: bone matrix and bone specific products*. Boston:

392   CRC Press, 1–78.

393   de Ricqlès AJ, Padian K, Horner JR, Lamm E-T, Myhrvold N. 2003. Osteohistology of

394   *Confuciusornis sanctus* (Theropoda: Aves). *Journal of Vertebrate Paleontology* 23(2):373-

395   386.

396   de Margerie E. 2002. Laminar bone as an adaptation to torsional loads in flapping flight. *Journal*

397   *of Anatomy* 201:521–526. DOI 10.1046/j.1469-7580.2002.00118.x.

398   de Margerie E, Cubo J, Castanet J. 2002. Bone typology and growth rates: testing and

399   quantifying 'Amprino's rule' in the mallard (*Anas platyrhynchos*). *Comptes Rendus*

400   *Biologies* 325:221–230. DOI 10.1016/S1631-0691(02)01429-4.

401   de Margerie E, Robin JP, Verrier D, Cubo J, Groscolas R, Castanet J. 2004. Assessing a

402   relationship between bone microstructure and growth rate: a fluorescent labelling study in the

403   king penguin chick (*Aptenodytes patagonicus*). *Journal of Experimental Biology* 207:869–

404   879. DOI 10.1242/jeb.00841.

405   de Margerie E, Sanchez S, Cubo J, Castanet J. 2005. Torsional resistance as a principal

406   component of the structural design of long bones: comparative multivariate evidence in birds.

407   *Anatomical Record* 282A:49-66.

408   Del Hoyo J, Elliot A, Sargatal J. eds. 1992. *Handbook of the Birds of the World*. Volume 1. Lynx

409   Edicions, Barcelona.

410   Enlow DH, Brown SO. 1958. A comparative histological study of fossil and recent bone tissues.

411   Part III. Mammalian bone tissues. General discussion. *Texas Journal of Science* 10:187-230.

412   Fowler ME. 1991. Comparative clinical anatomy of ratites. *Journal of Zoo Wildlife Medicine*

413   22:204-227.

414   Harshman, J, Braun EL, Braun MJ. 2008. Phylogenomic evidence for multiple losses of flight in

415   ratite birds. *Proceedings of the National Academy of Sciences of the United States of*

416   *America* 105:13462-13467.

417   Hernandez CJ, Majeska RJ, Schaffler MB. 2004. Osteocyte density in woven bone. *Bone*

418   35(5):1095-1099.

419   Hurvich CM, Tsai CL. 1989. Regression and time series model selection in small samples.

420   *Biometrika* 76:297-307.

421   Lee AH, Huttenlocker AK, Padian K, Woodward HN. 2013. Analysis of growth rates. In: *Bone*

422   *histology of fossil tetrapods: advancing methods, analysis, and interpretation*. Berkley:

423   University of California Press, 217-251.

424   Lee AH, Simons ELR. 2015. Wing bone laminarity is not an adaptation for torsional loading in

425   bats. *PeerJ* 3:e823. DOI 10.7717/peerj.823.

426   Legendre LJ, Bourdon E, Scofield, RP, Tennyson A, Lamrous H, de Ricqlès AJ, Cubo J. 2014.

427   Bone histology, phylogeny, and palaeognathous birds (Aves: Palaeognathae). *Biological*

428   *Journal of the Linnean Society* 112:688-700.

429   Lemaire V, Tobin FL, Greller LD, Cho CR, Suva LJ. 2004. Modeling the interactions between

430   osteoblast and osteoclast activities in bone remodeling. *Journal of theoretical biology*

431   229(3):293-309.

432   Makovicky PJ, Zanno LE. 2011. Theropod diversity and the refinement of avian characteristics.

433   In: *Living Dinosaurs*; *The Evolutionary History of Modern Bird*. Oxford: Wiley-Blackwell,

434   9-29.

435   Main RP. 2007. Ontogenetic relationships between in vivo strain environment, bone

436   histomorphometry and growth in the goat radius. *Journal of anatomy* 210:272-293.

437   Main RP, Biewener AA. 2007. Skeletal strain patterns and growth in the emu hindlimb during

438   ontogeny. *Journal of Experimental Biology* 20:2676-2690.

439   Marelli CA, Simons ELR. 2014. Microstructure and cross-sectional shape of limb bones in Great

440   Horned Owls and Red-tailed Hawks: how do these features relate to differences in flight and

441   hunting behavior? *PloS one* 9(8):e106094.

442   Maxwell EE, Larsson HCE. 2007. Osteology and myology of the wing of the emu (*Dromaius*

443   *novaehollandiae*), and its bearing on the evolution of vestigial structures. *Journal of*

444   *Morphology* 268:423-441. DOI: 10.1002/jmor.10527.

445   Maxwell EE, Larsson HCE. 2009. Comparative ossification sequence and skeletal development

446   of the postcranium of palaeognathous birds (Aves: Palaeognathae). *Zoological Journal of the*

447   *Linnean Society* 157:169–196.

448   Mescher AL. 2016. Bone. In: Mescher AL. ed. *Junqueira's Basic Histology, 14e.* New York,

449   NY: McGraw-Hill.

450   http://accessmedicine.mhmedical.com.mwu.idm.oclc.org/content.aspx?bookid=1687&Sectio

451   nid=109632699.

452   Mitchell KJ, Llamas B, Soubrier J, Rawlence NJ, Worthy TH, Wood J, Cooper A. 2014. Ancient

453   DNA reveals elephant birds and kiwi are sister taxa and clarifies ratite bird

454   evolution. *Science* 344(6186):898-900

455   Nagai H, Mak SS, Weng W, Nakaya Y, Ladher R, Sheng G. 2011. Embryonic development of

456   the emu, *Dromaius novaehollandiae. Developmental Dynamics* 240(1):162-175.

457   Ourfalian RM, Ezell K, Lee AH. 2016. Development of wing bone laminarity in the pigeon. *The*

458   *Official Journal of the Federation of American Societies for Experimental Biology*

459   30:779.12.

460   Padian K, de Ricqlès AJ, Horner JR. 2001. Dinosaurian growth rates and bird origins. *Nature*

461   412(6845):405-408.

462   Pratt IV, Cooper DML. 2017. A method for measuring the three-dimensional orientation of

463   cortical canals with implications for comparative analysis of bone microstructure in

464   vertebrates. *Micron* 92:32-38.

465   R Development Team. 2017. *R: A language and environment for statistical computing*. Vienna,

466   Austria: R Foundation for Statistical Computing.

467   Remeš V. 2007. Avian growth and development rates and age-specific mortality: the roles of

468   nest predation and adult mortality. *Journal of evolutionary biology* 20(1): 320-325.

469   Rubin CT, Lanyon LE. 1985. Regulation of bone mass by mechanical strain magnitude.

470   *Calcified tissue international* 37(4):411-417.

471   Sales J. 2007. The emu (*Dromaius novaehollandiae*): A review of its biology and commercial

472   products. *Avian and Poultry Biology Reviews* 18:1-20.

473   Shorter G. 2012. "Dromaius novaehollandiae". On-line, Animal Diversity Web.

474   http://animaldiversity.org/accounts/Dromaius_novaehollandiae/

475   Simons ELR, O'Connor PM. 2012. Bone laminarity in the avian forelimb skeleton and its

476   relationship to flight mode: testing functional interpretations. *The Anatomical Record*

477   295:386–396. DOI 10.1002/ar.22402.

478   Skedros JG, Hunt KJ, Hughes PE, Winet H. 2003. Ontogenetic and regional morphologic

479   variations in the turkey ulna diaphysis: implications for functional adaptation of cortical

480   bone. *The Anatomical Record* 273(1):609-629.

481   Skedros JG, Hunt KJ, Bloebaum RD. 2004. Relationships of loading history and structural and

482   material characteristics of bone: development of the mule deer calcaneus. *Journal of*

483   *morphology* 259(3):281-307.

484   Tjørve E, & Tjørve KM. 2010. A unified approach to the Richards-model family for use in

485   growth analyses: why we need only two model forms. *Journal of theoretical biology*

486   267(3):417-425.

487   van Gaalen SM, Kruyt M, Geuze RE, de Bruijn JD, Alblas J, Dhert WJ. 2010. Use of

488   fluorochrome labels in in vivo bone tissue engineering research. *Tissue Engering Part B:*

489   *Reviews* 16: 209-217.

490   Voeten DFAE, Cubo J, de Margerie E, Röper M, Beyrand V, Bureš S, Tafforeau P, Sanches S.

491   2018. Wing bone geometry reveals active flight in Archaeopteryx. *Nature Communications*

492   9(1):923.

493   Vogel S. 2013. *Comparative biomechanics: life's physical world*. Princeton University Press.

494   Warton DI, Hui FKC. 2011. The arcsine is asinine: the analysis of proportions in ecology.

495   *Ecology* 92(1):3-10.

496   Weiner S, Traub W, Wagner HD. 1999. Lamellar bone: structure-function relations. *Journal of*

497   *Structural Biology* 126:241-255.

498   Williams B, Waddington D, Murray DH, Farquharson C. 2004. Bone strength during growth:

499   influence of growth rate on cortical porosity and mineralization. *Calcified Tissue*

500   *International* 74:236-245.

501

502

Figure 1

Representative histological sections of emu femora, tibiotarsi, and humeri from a range of ages.

2.3 weeks (A, B, C), 8.1 weeks (D, E), 12 weeks (F), 16 weeks (G, H, I), 60 weeks (L), 416 weeks (J, K). Femora (A, D, G, J), tibiotarsus (B, E, H, K) and humeri (C, F, I, L). Scale bars equal 1000 µm for femora and tibiotarsi, and 250 µm for humeri. Bright field images of non-straightened caudal or medial octants (10x magnification).
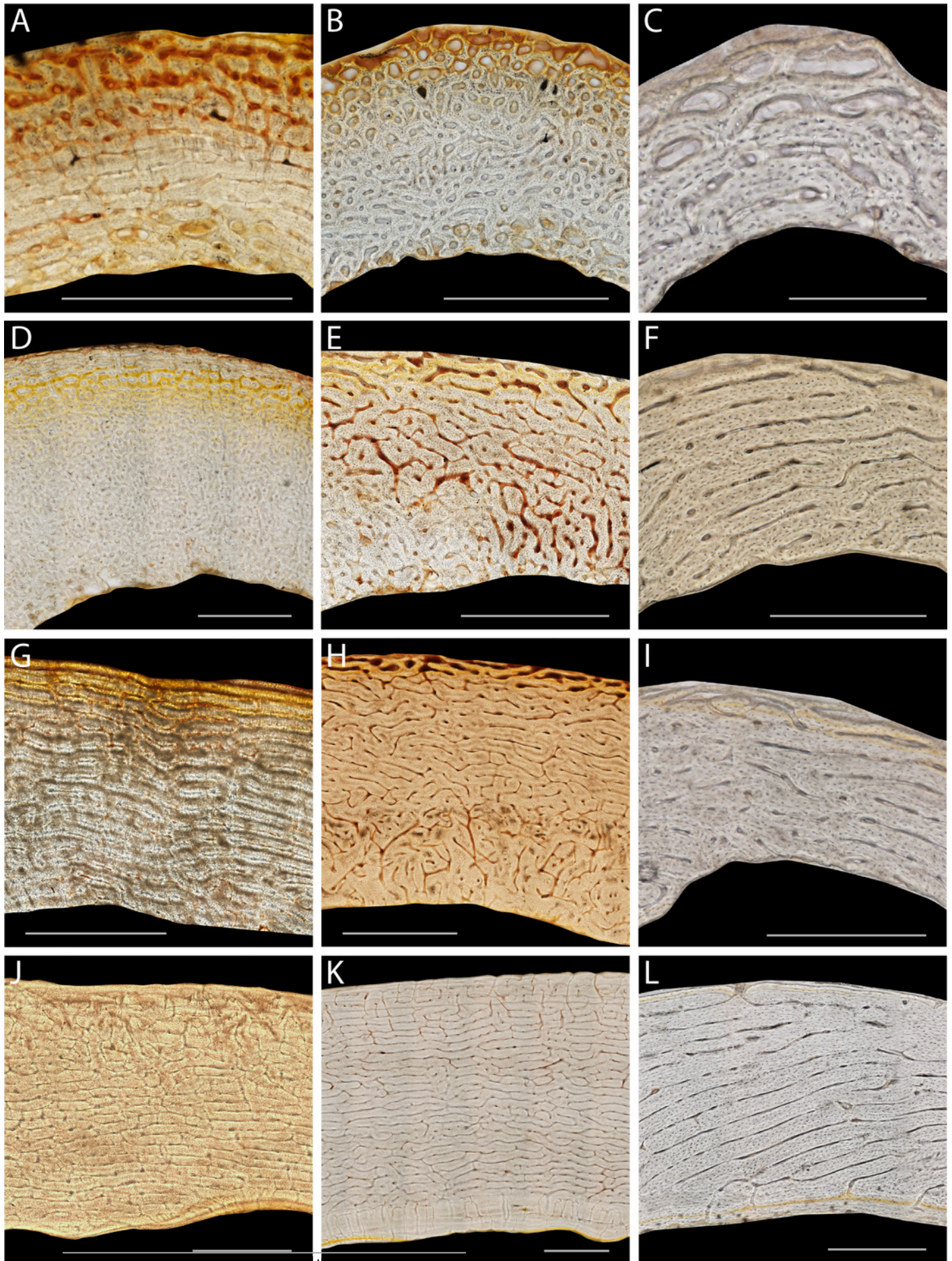
Figure 2

Histology of fluorescent-labelled bone.

On fluorescent images (A), the sample area was defined by outlining the periosteal extent of the xylenol (appears red) and calcein (green/yellow) tags. Growth rate was measured by taking the mean distance between consecutive fluorescent tags (white arrow) divided by number of days between injections. On brightfield images taken under the same magnification (B), laminarity was measured in the corresponding sample area.
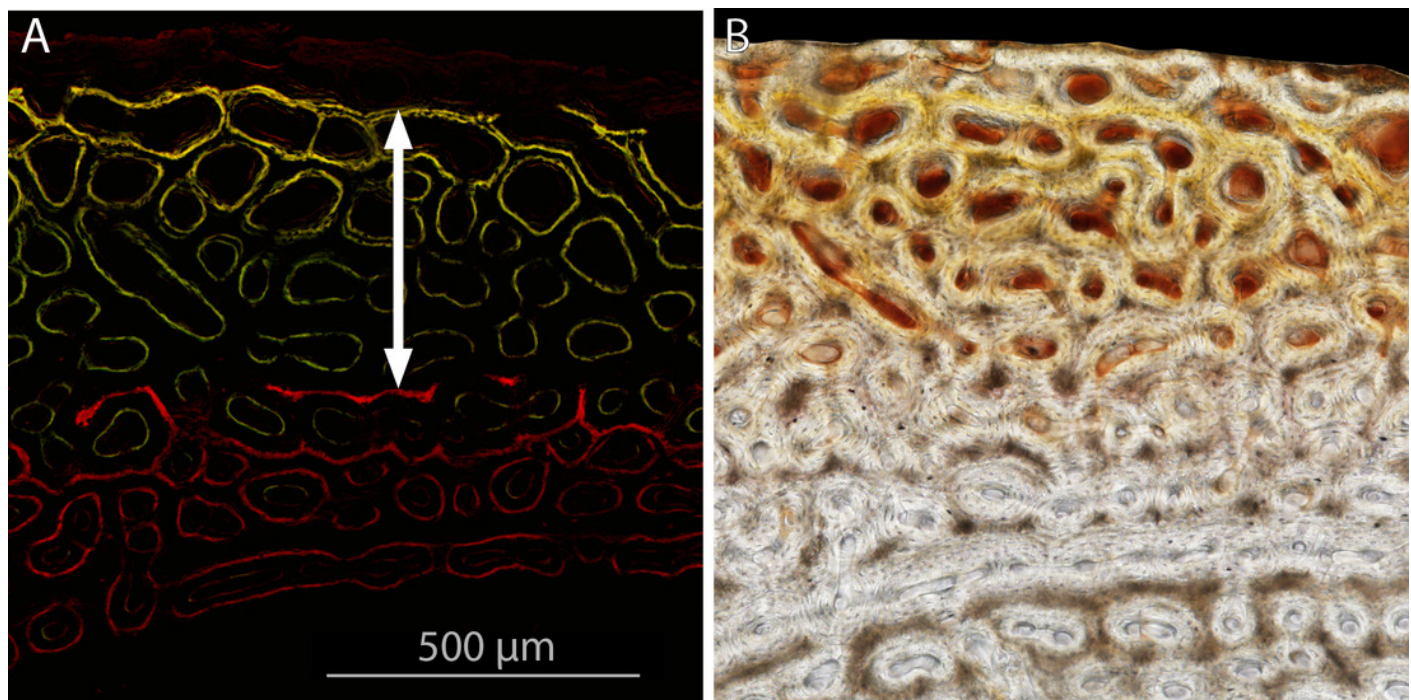
Figure 3(on next page)

Laminarity of the femur and tibiotarsus (tbt) plotted against growth rate.

Dark green and blue lines represent mean plot lines, shaded areas reflect 95% confidence interval bands. Logistic regression shows significant negative relationship (femur, p<0.001; tbt, p < 0.001; pseudo R^2 = 0.78). As growth rate increases, bone laminarity decreases. These results do not support the hypothesis that high laminarity is a result of fast growth rate in the emu hindlimb.
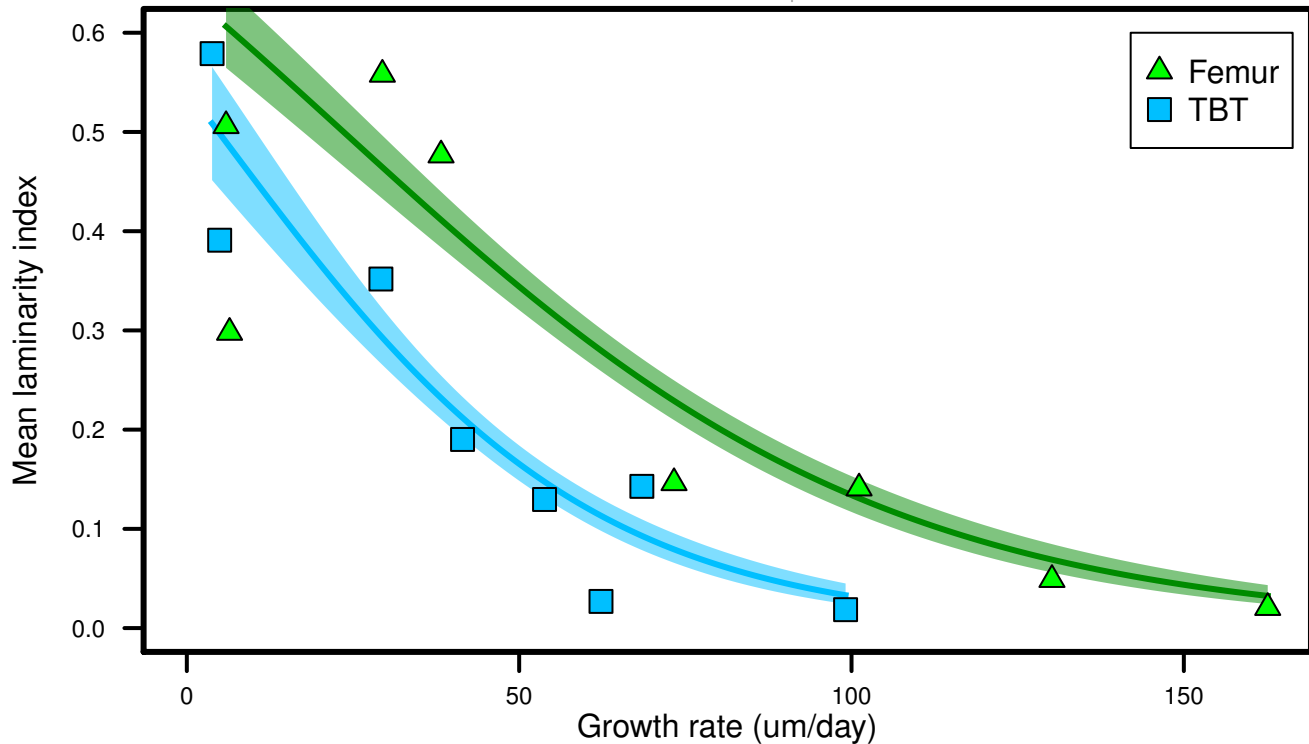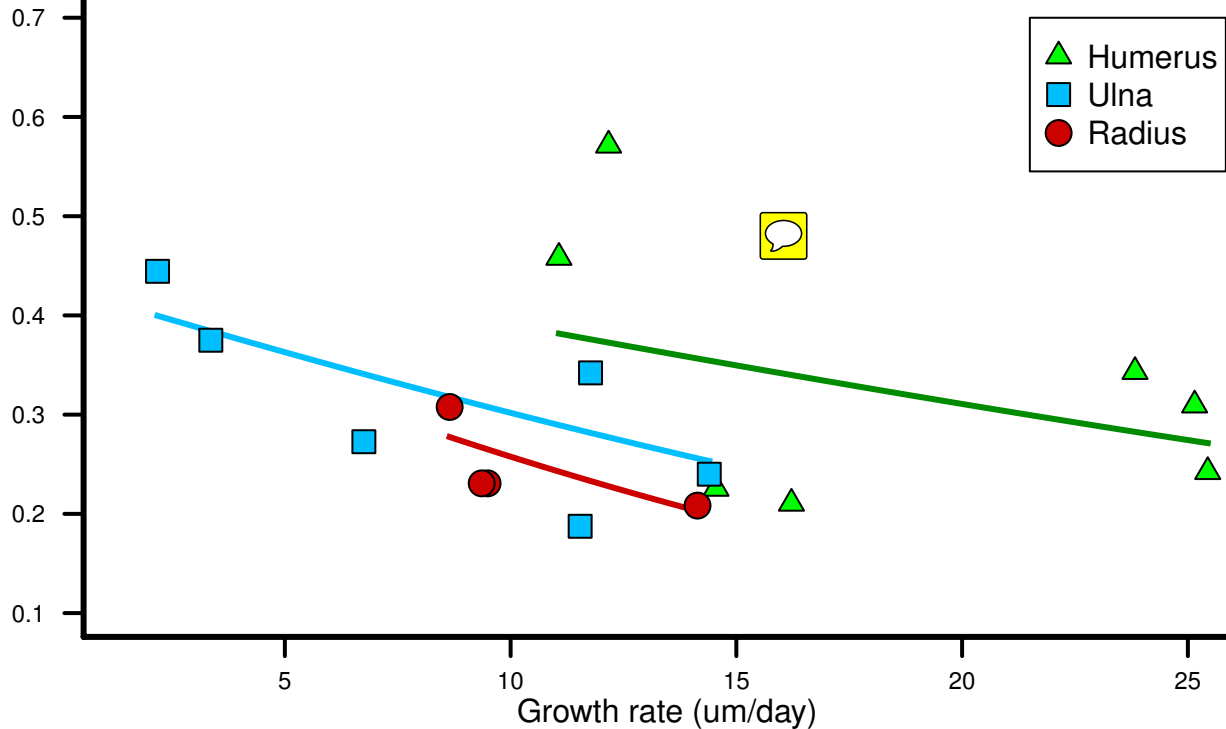
Figure 4(on next page)

Laminarity of the humerus, ulna, and radius plotted against growth rate.

Dark green, blue, and red lines represent mean plot lines. Logistic regression shows no significant relationship between laminarity and growth rate in wing elements (humerus: p=0.08, ulna: p=0.29, radius: p=0.52). These results do not support the hypothesis that high laminarity is a result of fast growth rate in the emu forelimb.

Figure 5(on next page)

Bone laminarity from the caudal octant of femur and tibiotarsus (tbt) plotted against shear strains measured at the caudal periosteal surface.

Dark green and blue lines represent mean plot lines, shaded areas reflect 95% confidence interval bands. Logistic regression shows significant positive relationship (femur: $p<0.001$; tbt: $p < 0.001$; pseudo $R^2 = 0.60$). As shear strain increases, bone laminarity increases. This result supports the hypothesis that high laminarity is a feature of bones experiencing greater shear strains.
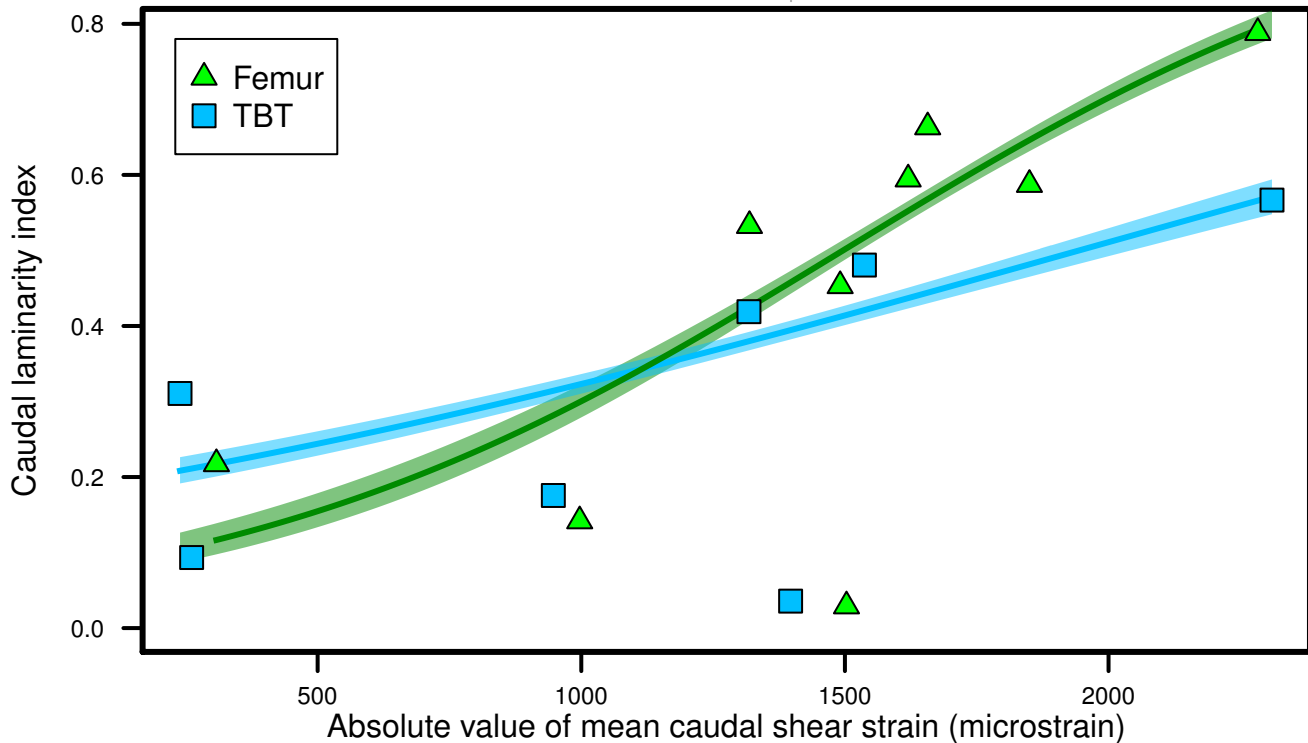
Table 1(on next page)

Emu identification number, age at sacrifice, and mass.

1

Specimen	Age (weeks)	Mass (kg)
15	2.3	0.74
1c	2.4	0.94
17	4.6	1.53
14b	8.1	4.73
16	12	6.85
2a	15.9	11.13
21	48	28.9
23	60.1	29.4
27	416	50.9
28	416	51.7

2

3

4

Table 2(on next page)

Growth rate and bone laminarity for specimens analyzed to address the growth hypothesis.

Laminarity Index (LI, calculated using the Wilson's estimate) was measured in a sample area outlined by the periosteal extent of two fluorescent tags. No growth was present in adult specimens #27 and 28. n/a indicates a specimen with no recorded circular canals.

1

Specimen	Age (weeks)	Element	Growth Rate (um/day)	LI
15	2.3	Femur	130.16	0.05
		Tibiotarsus	62.31	0.03
		Humerus	25.44	0.24
		Ulna	6.75	0.27
		Radius	15.22	0.20
1c	2.4	Femur	73.3	0.15
		Tibiotarsus	53.82	0.13
		Humerus	16.22	0.21
		Ulna	11.57	0.29
		Radius	9.49	0.25
17	4.6	Femur	162.62	0.02
		Tibiotarsus	99.11	0.02
		Humerus	25.15	0.31
		Ulna	11.54	0.19
		Radius	9.36	0.23
14b	8.1	Femur	101.14	0.14
		Tibiotarsus	68.46	0.14
		Humerus	23.83	0.34
		Ulna	14.4	0.24
		Radius	14.14	0.21
16	12	Femur	38.25	0.48
		Tibiotarsus	41.48	0.19
		Humerus	12.17	0.57
		Ulna	11.77	0.34
		Radius	8.65	0.31
2a	15.9	Femur	29.42	0.56
		Tibiotarsus	29.2	0.35
		Humerus	11.07	0.46
		Ulna	3.36	0.38
		Radius	2.37	0.29
21	48	Femur	6.43	0.30
		Tibiotarsus	4.94	0.39
		Humerus	14.55	0.23
		Ulna	2.18	0.44
		Radius	1.33	0.33

		Femur	5.9	0.51
23	60.1	Tibiotarsus	3.8	0.58
		Humerus	1.7	0.25
		Ulna	1.62	0.33
		Radius	1.67	0.40

2

Table 3(on next page)

Bone laminarity and caudal shear strain for specimens analyzed to address the biomechanical hypothesis.

Shear strain data was previously collected by Main and Biewener (2007). Laminarity Index (LI, calculated using the Wilson's estimate) was measured in four representative sample boxes (1.5 x 1.5 mm each) placed throughout the cortex on each caudal octant.

1

Specimen	Age (weeks)	Element	LI	Caudal Shear Strain (microstrain)
15	2.3	Femur	0.13	N/A
		Tibiotarsus	0.10	N/A
1c	2.4	Femur	0.22	-308
		Tibiotarsus	0.12	N/A
17	4.6	Femur	0.03	-1503
		Tibiotarsus	0.04	-1397
14b	8.1	Femur	0.14	-997
		Tibiotarsus	0.09	-261
16	12	Femur	0.45	-1491
		Tibiotarsus	0.18	-947
2a	15.9	Femur	0.59	-1620
		Tibiotarsus	0.31	-293
21	48	Femur	0.66	-1657
		Tibiotarsus	0.42	-1318
23	60.1	Femur	0.79	-2283
		Tibiotarsus	0.55	N/A
27	416	Femur	0.53	-1319
		Tibiotarsus	0.48	-1537
28	416	Femur	0.59	-1850
		Tibiotarsus	0.57	-2310

2

3